Structural and vibrational properties of carbon monoxide adlayers on the copper (001) surface

Steven P. Lewis[a] and Andrew M. Rappe[b]
Department of Chemistry and Laboratory for Research on the Structure of Matter, University of Pennsylvania, Philadelphia, Pennsylvania 19104

(Received 10 July 1998; accepted 26 October 1998)

The structure and vibrational states of a prototype adsorbate-substrate system—carbon monoxide on the copper (001) surface—have been calculated from first principles within local density functional theory. Three CO coverages have been examined: $\theta=0$ (bare surface), 0.5, and 1. These systems are represented by a well converged slab model within which all atomic degrees of freedom are treated on an equal footing. The computed structural relaxations and vibrational frequencies are generally in excellent quantitative agreement with the available experimental measurements. The full monolayer is found to be energetically favorable to the half monolayer plus free CO molecule. This indicates that the maximum stable coverage is greater than $\theta=0.5$, in agreement with experiment. The vibrational analysis reveals that resonant coupling between adsorbate and substrate motions has a profound effect on the vibrational spectra, for example, the low-frequency, in-plane frustrated translational motion of the CO molecules mixes with long-wavelength copper phonons to form a broad resonance peak. This implies a finite lifetime which, for the half-monolayer system, is computed to be 3.0 ps, in excellent agreement with the measured value of 2.3 ± 0.4 ps. For the full-monolayer system, the predicted lifetime is 0.7 ps; however this system is presently inaccessible to experiment. Resonant coupling is also found to affect the Rayleigh wave of the copper (001) surface. At half-monolayer CO coverage, this mode resonantly mixes with bulk copper phonons developing a finite lifetime, which is predicted to be 5.2 ps. To our knowledge, the lifetime of this mode has never been measured. For the fully covered surface, the Rayleigh wave does not form a resonance because the phonon coupling is forbidden by symmetry. © *1999 American Institute of Physics.* [S0021-9606(99)70305-3]

I. INTRODUCTION

The interactions between molecules and metal surfaces are fundamental to surface chemistry. They play a critical role in many important applied phenomena, including catalysis, corrosion, and materials growth.[1] In order to enhance and control surface processes with greater precision, research in this field has begun in recent years to focus on developing a microscopic understanding of the nature and consequences of molecule–surface interactions.

One of the most striking consequences of these interactions is the emergence of new vibrational modes associated with fluctuations of the chemisorption bond. These modes have no vibrational counterpart in either component separately. Rather, they correspond to the translational and rotational degrees of freedom of the free molecules, which become ''frustrated'' upon attachment to the substrate. These vibrations are generally low-energy excitations that are thermally populated in many experimental situations. As a result, they are instrumental in a wide variety of physical and chemical processes at surfaces, including reactivity, energy dissipation, and molecular diffusion and desorption.

In this article we report an in-depth, state-of-the-art theoretical analysis of the microscopic structure and vibrational properties of a prototypical chemisorbed metal: carbon monoxide on the (001) surface of copper. This system has several attractive features that have made it the subject of considerable experimental[2–11] and theoretical[12–20] interest in recent years. It exhibits many of the interesting physical properties unique to chemisorbed metals without possessing the obscuring detail of more complex systems. In particular, the simplicity of CO and of the copper (001) surface, as well as the high symmetry of the chemisorbed overlayer, facilitate theoretical and experimental investigation of this system. Furthermore, this system is comparatively easy to prepare in the lab and is stable over long periods of time, thereby permitting detailed experimental investigations. Finally, the CO–copper system is of intrinsic interest because of its vital role both as a prototype and as a direct participant in important catalytic processes (e.g., methanol production).[1]

The first-principles investigation presented here provides, to our knowledge, the first unbiased, systematic, and quantitative theoretical study of the vibrational properties of an adsorbed metal surface in which all parts of the system are treated on an equal footing. Up until now, the vibrational properties of these systems have been characterized solely by atomic motions localized at the adsorbates, with the substrate (except perhaps the top layer) treated as a rigid platform against which the molecules oscillate. We have taken the

[a]Present address: Dept. of Physics and Astronomy, University of Georgia, Athens, GA 30602-2451.
[b]Electronic mail: rappe@sas.upenn.edu

point of view that coupling between the molecules and the substrate can alter this simple picture in very important ways, and thus have carried out our analysis in a theoretical framework broad enough to incorporate bulk and surface degrees of freedom as well as those of the adsorbate. As a result, we have been able to show that coupling between the adsorbate overlayer motion and the substrate phonons plays a dominant role in the rapid relaxation observed for the in-plane frustrated translation of CO on copper (001) at half coverage.[5]

In Sec. II we describe in depth the systems being studied. Details of the computational methodology are provided in Sec. III, and a careful analysis of the convergence properties of the calculations is provided in Sec. IV. In Secs. V and VI the results of the structural and vibrational analyses, respectively, are reported. Finally, the investigation is summarized in Sec. VII.

II. DESCRIPTION OF SYSTEMS

In this study we compare the structural and vibrational properties of three systems: (a) the clean (001) surface of the face-centered-cubic (fcc) metal, copper, (b) an ordered overlayer of carbon monoxide molecules on the copper (001) surface in which half of the surface copper atoms are covered, and (c) an ordered overlayer in which all surface sites are covered. In terms of the surface coverage parameter, θ, these systems correspond to $\theta=0$, 0.5, and 1 monolayers (ML), respectively. Of these three, only the first two are experimentally observed. Experiment has shown that CO saturates the copper (001) surface at 0.57 ML.[21,22] Thus the $\theta=1$ system is, at present, only hypothetical. We include it in this study in order to examine coverage-dependent properties. Other adlayers with $\theta<0.5$ would require unit cells containing too many atoms for current accurate, first-principles methods, because of their long repeat distances in the plane.

The ideal $\theta=0$ system consists of a semi-infinite expanse of bulk fcc copper separated from a semi-infinite expanse of vacuum by the (001) surface at the plane $z=0$. Each (001) copper layer consists of a square planar array of atoms with repeat distance $a/\sqrt{2}$, where a is the conventional fcc lattice constant of copper. These layers are stacked along the z axis with an $ABAB\ldots$ stacking sequence, where atoms in B layers are situated directly above the square hollow sites of A layers, and vice versa. This system has C_{4v} point symmetry about the z axis and a primitive surface unit cell containing one atomic site.

Carbon monoxide adsorbs to the copper (001) surface with the carbon end bound to a surface copper atom at the so called ''top site'' and with the molecular bond oriented normal to the surface.[23,24] At half-monolayer coverage, the adlayer has an ordered structure with centered 2×2 symmetry relative to the bare (001) surface.[21] This structure, depicted in Fig. 1(a), has C_{4v} point symmetry, with every covered surface atom fourfold coordinated by bare surface atoms, and vice versa. The primitive surface unit cell, $(\sqrt{2}\times\sqrt{2})R45°$, is a square of side a rotated 45° relative to the bare-surface unit cell and containing two inequivalent sites, one covered and one empty. The two sites are located at the corner and at the center of the unit cell, respectively, for A layers, and at points [0,1/2] and [1/2,0] (in lattice units), respectively, for B layers. We have adopted a labeling convention whereby, in any given layer, atoms at the two inequivalent sites are distinguished by whether or not their label has a prime [see Fig. 1(c)]. Specifically, atoms at or below the covered (empty) site are unprimed (primed). Copper layers are numbered consecutively starting with the surface layer.

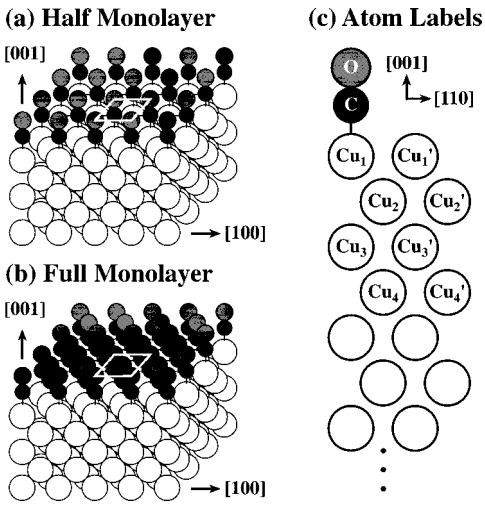

FIG. 1. Illustration of the structure of CO on copper (100) at (a) half coverage and (b) full coverage. A $\sqrt{2}\times\sqrt{2}R45°$ surface unit cell is outlined in white in both (a) and (b). The atomic labeling convention used throughout this article is shown in (c).

The hypothetical $\theta=1$ system is illustrated in Fig. 1(b). It consists of an ideal (001) copper substrate with every surface atom covered by a CO molecule. This system has the same symmetry as the bare surface.

The structural and vibrational analyses reported below have been carried out using the $(\sqrt{2}\times\sqrt{2})R45°$ surface unit cell for *all three* systems. Even though this cell is primitive only for the half-covered surface, we have made this choice in order to facilitate comparisons and to guarantee that all calculations are of equal precision. For computational convenience, the convergence tests reported in Sec. IV involving surface calculations are based on the bare surface using the primitive, one-site unit cell. Further test calculations show that the two-site cells have analogous convergence properties.

III. COMPUTATIONAL METHODOLOGY

Determining structural and vibrational properties involves calculating the ground-state total energy and atomic forces for many different configurations of the atoms. We compute these quantities with quantum-mechanical accuracy using density functional theory[25,26] (DFT). Our code efficiently solves the DFT problem using the conjugate-gradient method to minimize the energy functional with respect to the electronic degrees of freedom.[27–29] The DFT exchange and correlation energies are treated in this study within the local density approximation[30] (LDA). A recent comparative study showed that the LDA and the generalized gradient approximation[31] (GGA) give comparable values for the

TABLE I. Parameters used in generating pseudopotentials for copper, carbon, and oxygen. The pseudopotentials were generated using the method of Ref. 36.

Element	Copper (+1)			Carbon		Oxygen	
Angular momentum	*s*	*p*	*d*	*s*	*p*	*s*	*p*
Reference configuration	0.75	0.25	9.00	2.00	2.00	2.00	4.00
r_c (a.u.)	1.70	1.90	2.00	1.30	1.30	1.30	1.40
q_c (a.u.)	5.50	5.50	7.10	6.50	7.10	6.50	7.10

structural parameters and vibrational frequencies of CO on copper (001).[16] Atomic forces are computed using the Hellmann–Feynman theorem.[32]

The calculations use a well-converged plane-wave basis set to represent the Kohn–Sham single-particle wave functions[33,34] and *ab initio*, norm-conserving pseudopotentials[35] to describe the interaction of valence electrons with the ion cores of copper, carbon, and oxygen. We have followed the formulation of Ref. 36 to generate pseudopotentials optimized to require as few plane waves as possible, while maintaining excellent total-energy convergence. This procedure involves minimizing the kinetic energy contained in Fourier components larger than a specified cutoff wave vector, q_c, subject to various constraints. The cutoff wave vector is chosen so that $q_c^2 \leqslant 2mE_c/\hbar^2$, where E_c is the energy cutoff of the plane-wave basis. The resulting nonlocal pseudopotentials are then put in fully separable form.[37,38] In this work we have not included relativistic corrections to the atomic Hamiltonian in generating the pseudopotentials. Their inclusion has been shown to have only a slight effect on the structural properties of copper.[39]

The three systems under investigation are represented in the calculations by a structural model in which the semi-infinite copper (001) substrate is truncated to a slab of finite thickness. The truncation error is systematically reduced by increasing the thickness of the slab until the properties calculated converge. Each model system is described by a periodically reproduced supercell,[40] which captures the periodicity and infinite extent of the true system parallel to the surface. The effects of the artificial periodicity perpendicular to the surface are made negligible by including a sufficiently thick layer of vacuum in the supercell to isolate adjacent slabs. For the $\theta = 0.5$ and 1 systems, we place the CO molecules on both the top and bottom surfaces of the slab. This gives the system inversion symmetry, which facilitates many aspects of the calculation and speeds up the self-consistency. The point symmetry of all three unit cells is D_{4h}.

Integrations over the surface Brillouin zone (SBZ) are approximated in the calculations by sums over a discrete mesh of special *k* points.[41] This discretization can be problematic for metals, since a dense *k*-point sampling is required to resolve Fermi surface details. These difficulties are dramatically reduced, however, by performing the calculations at finite electronic temperature, using the Mermin functional to describe the electronic free energy.[42] This has the effect of broadening each single-particle energy level into a peak of finite width, thus permitting fractional occupations (i.e., $0 \leqslant f_i \leqslant 1$). One consequence of this approach is that the filling factors become nontrivial variables in the energy-minimization procedure and must be updated appropriately. We have adopted the procedure of Gillan[27] for handling this issue.

IV. CONVERGENCE TESTING

In Sec. III several approximations that are made in the calculations were described. Most of these are controlled approximations, controlled in the sense that the exact limit can be achieved by systematically varying one or more parameters. Choosing the operating values of these parameters for complicated systems such as adsorbed metal surfaces often requires striking a delicate balance between quantitative accuracy and computational tractability. Therefore, we have carefully tested the convergence behavior of the calculations with respect to variations of the control parameters. The results are presented in detail in the following.

The first step in designing pseudopotentials is to partition the electrons into valence and core states. This approximation can be systematically improved by transferring additional shells of electrons from the core to the valence manifold until the results converge. In many atoms the core-valence partitioning is uncontroversial. For carbon and oxygen, the $2s$ and $2p$ electrons both participate in chemical bonding, whereas the $1s$ electrons are more than 18 Ry lower in energy and remain chemically inert. For copper, on the other hand, there is some ambiguity. Since the ground-state electron configuration of copper is $3d^{10}4s^1$, it might seem natural to include the closed $3d$ shell in the core, leaving only one valence electron. However, while this is very appealing computationally, it leads to a poor description of copper, since the $3d$ and $4s$ levels have comparable energies and thus mix in most chemical environments. A minimum of 11 valence electrons is required, therefore, for a correct description of copper, making calculations involving this element computationally very demanding. Indeed, one might argue that the copper $3s$ and $3p$ states should also be treated as valence states, as they are only a few Ry lower in energy than the oxygen $2s$ state. However, the introduction of eight new valence electrons per copper atom would significantly increase the computational cost, and have only a marginal effect on the accuracy. As we show below, the bulk and surface properties of copper are very accurately described by including only the 11 outer electrons in the valence manifold.

The reference configurations, cutoff radii, and cutoff wave vectors used to generate the optimized pseudopotentials[36] for copper, carbon, and oxygen are compiled in Table I. For carbon and oxygen, the neutral, ground-

TABLE II. Transferability tests for the Cu pseudopotential. The valence eigenvalues and the total energies from pseudopotential calculations are compared to all-electron values for test configurations in three charge states around the reference configuration. The total energies are measured relative to the total energy in the reference configuration.

Test configuration	Charge (e)	Eigenvalue error (%)			E_{tot} error (meV)
		s	p	d	
$s^{1.5}d^{9.5}$	0.0	−0.60	+0.31	−2.04	−54
$s^{1.0}d^{9.5}$	+0.5	−0.66	−0.35	−1.06	−46
$s^{0.5}d^{9.0}$	+1.5	−0.01	−0.01	+0.25	0

state configuration is chosen as reference, whereas the copper reference configuration is a +1 ionized state. The pseudopotentials for all three species are generated to be optimally convergent for a 50 Ry plane-wave basis. A large number of plane waves is required for these atoms because elements in the $2p$ row (e.g., carbon and oxygen) and the $3d$ row (e.g., copper) lack p and d states, respectively, in the core, resulting in fairly sharply peaked valence states. The cutoff radii are chosen to be as small as possible while still giving a convergence error less than about 15 meV/atom and no ghost states.[38]

The transferability of each pseudopotential to different chemical environments has been tested by computing the total energy and the Kohn–Sham eigenvalues for an isolated atom in a variety of charged and excited-state configurations around the reference state, and then comparing these values to those computed using all of the electrons. Table II displays representative results of these test calculations for the copper pseudopotential. Since pseudopotential and all-electron calculations have different zeros of energy, all total energies are measured relative to the reference configuration. We see from Table II that the copper pseudopotential has good transferability over the range of configurations tested. Not surprisingly, the least transferable component is the d angular momentum channel. This is a common characteristic of pseudopotentials for $3d$ transition metals. Recent advances in the design of nonlocal pseudopotentials, however, promise to significantly improve pseudopotential transferability across the Periodic Table, including the $3d$ row.[43] Tests on the carbon and oxygen pseudopotentials show them to have even better transferability properties than copper.

To test the accuracy of the pseudopotentials, we have used them to compute the structural and cohesive properties of simple bulk materials. Table III presents the results for bulk copper, computed using two different unit cells: the two-atom tetragonal Bain cell of the fcc structure[44] as well as the primitive fcc cell. We include the former because it has the same symmetry as the fcc (001) surface, and we have found that this symmetry consistency leads to fruitful error cancelations when comparing bulk and surface calculations (see below). For the Bain cell calculations, the Brillouin zone is sampled on an $8\times8\times6$ mesh (30 irreducible k points), whereas the primitive fcc calculations use a k-point grid comprising 28 irreducible points. Energy levels are broadened to a width of 0.05 eV. For comparison, Table III also includes the results of previous LDA calculations as well as those of experiment. The previous calculations cited include pseudopotential studies using a mixed basis (PP-MB),[46] a plane-wave basis (PP-PW),[47] and a Gaussian-type-orbital basis (PP-GTO),[48] as well as all-electron studies using the linear augmented plane-wave (LAPW) method[39] and the Korringa–Kohn–Rostoker (KKR) method.[49]

TABLE III. Structural properties of bulk copper. Results from the present pseudopotential study were obtained with a 50 Ry plane-wave basis for two different fcc unit cells: the two-atom, tetragonal Bain cell and the standard primitive cell. See the text for details. Results from a number of previous calculations [both nonrelativistic (NR) and scalar relativistic (SR)] and experiment are provided for comparison.

Study	a (Å)	E_{coh} (eV/atom)	B (GPa)
Present study			
Bain cell (NR)	3.599	4.154	165
Primitive cell (NR)	3.601	4.134	162
Previous theory			
PP-MB (NR)[a]	3.62	3.61	147
PP-PW (NR)[b]	3.60	4.19	160
PP-PW (SR)[b]	3.57	4.38	174
PP-GTO (SR)[c]	3.62	3.83	188
LAPW (NR)[d]	3.61	4.14	162
LAPW (SR)[d]	3.56	4.42	183
KKR (NR)[e]	3.58	4.10	152
Experiment	3.61[f]	3.50[g]	142[h]

[a]Reference 46.
[b]Reference 47.
[c]Reference 48.
[d]Reference 39.
[e]Reference 49.
[f]Reference 50.
[g]Reference 51.
[h]Reference 52.

The lattice constant, cohesive energy, and bulk modulus of copper computed using our 50 Ry pseudopotential are in excellent agreement with the other nonrelativistic LDA calculations. Particularly noteworthy is the comparison to the LAPW calculation of Ref. 39. Since that study was an all-electron calculation, the close agreement between the two sets of results indicates an absence of any significant pseudopotential error in our calculations. Furthermore, the agreement with experiment is within the range expected for LDA calculations for all three quantities reported. Similarly good agreement with experiment and previous theory is also found in bulk calculations using the carbon and oxygen pseudopotentials.

TABLE IV. Convergence with respect to vacuum-layer thickness. Calculations are for a three-layer slab with the experimental in-plane lattice constant. ΔE is the difference in energy between the bulk-terminated surface and a 3% inward relaxation. Vacuum thickness, N_v, is given in units of the (001) interlayer spacing of bulk copper (1.80 Å).

N_v	ΔE (meV/surface)
3	5.924
5	5.943
7	5.920
9	5.906
13	5.900

TABLE V. Relaxed interlayer spacings and surface energies for copper (001) slabs of varying thicknesses. The calculations used a 4×4 k-point grid in the SBZ and a 12.5 Å vacuum layer between slabs. Note: For convergence testing, the in-plane lattice constant was set to the experimental value. Thus the data here *are not* LDA predictions for the copper (001) surface relaxations (see Table VIII).

N_s	5	7	9
d_{12} (%)	−2.60	−2.89	−2.82
d_{23} (%)	0.28	0.65	0.60
d_{34} (%)	⋯	0.04	0.12
d_{45} (%)	⋯	⋯	0.41
E_{surf} (eV)	0.780	0.800	0.810

TABLE VI. Surface relaxations and energy as a function of k-point sampling for a five-layer copper (001) slab. The k-point set designations refer to sampling in the (001) plane. Sampling perpendicular to this plane was restricted to one sheet of k points at $k_z=0.25$ in reciprocal-lattice units. The calculations were performed using the experimental value for the surface lattice constant. See the text for details.

k-point set (Irreducible k points)	4×4 (3)	6×6 (6)	8×8 (10)	10×10 (15)
d_{12} (%)	−2.60	−2.97	−2.99	−2.93
d_{23} (%)	0.28	0.43	0.20	0.22
E_{surf} (eV)	0.780	0.782	0.759	0.766

Making the slab approximation in surface calculations introduces two new convergence parameters: vacuum thickness and slab thickness. Table IV contains the results of our vacuum convergence testing. We have computed, as a function of vacuum-layer thickness, the energy difference between a three-layer copper slab with bulk interlayer spacings and one with 3% inward relaxation of the two surfaces. This magnitude of relaxation is typical of low-index metal surfaces. Vacuum thickness is given in units of the bulk (001) interlayer separation, about 1.8 Å. The results show that the energy difference fluctuates by less than 1% for all vacuum-layer thicknesses tested, indicating a weak dependence on this parameter. We have chosen an operating value of seven layers, or about 12.5 Å of vacuum separating neighboring slabs. For calculations of the adsorbed surface, the vacuum is measured from the outer edge of the adsorbate.

To test the convergence with respect to slab thickness, we have computed the fully relaxed structure and surface energy of five-, seven-, and nine-layer copper slabs. All layers of atoms were free to move in the relaxations. The in-plane lattice constant was set to the experimental bulk value, and the SBZ was sampled on a 4×4 mesh containing three irreducible k points. Relaxed interlayer spacings are reported as percent deviations from the bulk value. We have found that great care must be taken in comparing slab and bulk interlayer spacings. For the true bulk material, fcc symmetry fixes the (001) interlayer spacing at $a/2$. However, the reduced symmetry of the slab unit cell removes this constraint, allowing the spacing to relax away from the ideal value, even in the bulk-like region. Therefore, to make a fair comparison, it is necessary to determine the bulk spacing in a manner that is consistent with the slab calculations. We have studied bulk copper in the tetragonal Bain cell using the same in-plane lattice constant and in-plane k-point grid as in the slab calculations, and find that the relaxed interlayer spacing is 1% smaller than the ideal fcc value. We use this bulk spacing in evaluating surface relaxations. For the calculations to be completely internally consistent, we should also relax the in-plane lattice constant of the Bain cell for a given k-point set and use that value in both bulk and slab calculations.[45] We *have* followed that procedure for the structural and vibrational analyses that follow. However, for judging slab-thickness and k-point convergence, it is sufficient to fix the in-plane lattice constant at the experimental value.

The slab-thickness convergence tests are summarized in Table V. The notation d_{ij} refers to the relaxed spacing between layers i and j, and E_{surf} denotes the surface energy, defined as $E_{\text{surf}}=(N_sE_{\text{bulk}}-E_{\text{slab}})/2$, where N_s is the number of atomic layers in the slab. The tabulated results show that the seven- and nine-layer slabs are in excellent agreement with each other, whereas the five-layer slab differs somewhat. Even though the five-layer slab is not horribly unconverged, we have chosen to proceed in our investigations of CO-adsorbed copper using a slab containing seven copper layers since the added computational cost is not prohibitive.

To assess the k-point convergence behavior of the calculations, we have computed the fully relaxed structure and surface energy of a five-layer copper slab for four k-point meshes: 4×4, 6×6, 8×8, and 10×10. The relaxations were performed using the experimental in-plane lattice constant. Thus, for the 4×4 k-point set, the resulting interlayer spacings are compared to the relaxed bulk value, as described above. For the other three k-point sets, we find that the relaxed bulk interlayer spacing differs only negligibly from the ideal value. Table VI shows that *all four* k-point sets give very similar surface relaxations and energies. While the larger k-point sets are somewhat better converged, these results indicate that the 4×4 mesh is a reasonable choice for our further slab calculations, provided comparisons to bulk are done correctly. This is extremely advantageous since the next larger mesh, 6×6, would *double* the computational effort.

For calculations involving the $(\sqrt{2}\times\sqrt{2})R45°$ surface unit cell, the 4×4 k-point mesh in the SBZ of the bare surface gets folded onto a set of eight k points in the new SBZ. This set has two irreducible k points.

Unless noted otherwise, all calculations in this study used an energy-level broadening width of 0.30 eV. Test calculations on bulk copper show that structural and vibrational

TABLE VII. Summary of the convergence parameters used throughout this study.

Parameter	Value
Plane-wave cutoff (E_c)	50 Ry
Slab thickness (N_s)	7 layers
Vacuum thickness	12.5 Å
SBZ sampling (one-site cell)	4×4 mesh
Irreducible (one-site cell)	3 k points
Irreducible (two-site cell)	2 k points
Energy level broadening (w)	0.3 eV

TABLE VIII. Computed structural and energetic properties of bulk copper, the clean copper (001) surface, and a free CO molecule. For the surface, interlayer spacings are reported both as a percentage change from the bulk value and in Å. The bulk data were obtained using the Bain cell and the same 4×4 in-plane k-point grid as is used in the surface calculations. See the text for further explanation.

Quantity	Theory	Experiment
	(a) Bulk copper	
a (Å)	3.592	3.61[a]
$d_{(001)}$ (Å)	1.796	1.805
E_{coh} (eV/atom)	4.21	3.50[b]
B (GPa)	170	142[c]
	(b) Copper (001) surface	
d_{12} [% (Å)]	−1.38 (1.771)	−(1.2–2.4)[d]
d_{23} [% (Å)]	0.60 (1.807)	0.0–1.0[d]
d_{34} [% (Å)]	−0.02 (1.795)	
E_{surf} (eV)	0.819	0.82[d]
	(c) Free CO molecule	
d_{bond} (Å)	1.123	1.128[e]
ν (cm^{-1})	2173	2143[f]

[a]Reference 50.
[b]Reference 51.
[c]Reference 52.
[d]Reference 46, and references therein.
[e]Reference 53.
[f]Reference 54

properties are largely insensitive to this parameter over the range of values tested (0.05–0.30 eV). The main difference is that the calculations achieve self-consistency somewhat faster with a larger broadening width. Table VII contains a summary of the convergence parameters that are used throughout this investigation.

V. STRUCTURAL ANALYSIS

Equilibrium structures of the bare, half-covered, and fully covered copper (001) surface have been computed using the methodology described in Sec. III. This analysis provides important information regarding the nature of the interactions at the surface and is an essential first step in determining the vibrational states. In these relaxations, we have allowed all atoms of the slab to move, and have deemed the structure to be relaxed when all atomic forces are smaller in magnitude than 0.01 eV/Å. At this point, the copper atoms (which have the softest degrees of freedom) are within a few thousandths of an angstrom of their zero-force positions.

Structural relaxations for these systems only involve atomic motions perpendicular to the surface. Since all atoms occupy sites of fourfold symmetry about the z axis, the in-plane atomic coordinates are all at local extrema. The only in-plane degree of freedom left to be determined is the dimension of the surface unit cell, which is equal to the bulk lattice constant. We saw in Sec. IV that it is important to determine this value in a manner consistent with the surface calculations. Thus, we have computed the ground-state structural properties of bulk copper using the tetragonal Bain cell and a $4\times4\times12$ k-point grid. The results are summarized in Table VIII(a). All surface calculations reported below have been carried out using an in-plane lattice constant of 3.592 Å.

The relaxed structure and energetics of the bare (001) surface are given in Table VIII(b). Surface relaxation of metals is a subtle effect. The atoms move only a small distance from their bulk positions, and the relaxation energy per unit cell (i.e., half the difference in energy between the bulk-terminated and fully relaxed slab) is only about 1% of the surface energy per unit cell. The relaxation shows an oscillating pattern in which d_{12} is an inward relaxation and d_{23} is outward. This pattern is typical of metals and is associated with a one-dimensional Friedel oscillation along the z axis induced by the presence of the surface. By the third pair of (001) layers, the oscillation has largely died out, with the interlayer spacing almost at the bulk value. The computed spacings all fall within the range of the experimental values, which have been measured using several different techniques.[46] Furthermore, the surface energy is also in excellent agreement with experiment.

For completeness, we have also computed the properties of a free CO molecule, as shown in Table VIII(c). The values computed for the bond length and the vibrational frequency agree closely with those of experiment. This information is important for judging the effect of adsorption.

Table IX reports the relaxed structure and adsorption energy of the half-covered and fully covered surfaces. The adsorption energy is defined as the adsorbate binding energy

TABLE IX. Equilibrium structure and adsorption energy for full and half monolayers of CO on the copper (001) surface. The structure is reported as the vertical distance between layers of atoms. For $\theta=0.5$, there are two distinct sites per surface unit cell. These are referred to as covered and empty, depending on whether or not the atom is below a CO molecule.

	Separation (Å) $\theta=0.5$				
	Present study				
Layer pairs	Covered	Empty	Previous calc.[a]	Experiment	$\theta=1$
O–C	1.138		1.14	1.15±0.10[b]	1.136
C–Cu_1	1.852		1.88	1.92±0.05[c]	1.882
Cu_1–Cu_2	1.805	1.768			1.815
Cu_2–Cu_3	1.804	1.821			1.815
Cu_3–Cu_4	1.809	1.792			1.796
E_{ads} (eV/CO)	1.239		1.51	0.57[d]	0.695

[a]Reference 16.
[b]Reference 23.
[c]Reference 24.
[d]Reference 21.

per molecule measured relative to the bare surface and the free molecule. Since the $\theta=0.5$ system has two inequivalent sites per surface unit cell, distinct copper interlayer spacings are reported for both. In the $\theta=1$ system, both sites are equivalent by symmetry. The computed structure of the half-covered surface is in excellent quantitative agreement with the available experiments and a previous calculation (see Table IX for citations). Previous results do not exist for the hypothetical fully covered surface.

For both coverages, adsorption has a similar effect on the local structure of the component systems. The adsorbed CO molecule is 1.2% longer than free CO, and the Cu_1–Cu_2 spacing at the binding site actually *expands* relative to the bulk by 0.5%–1%, in contrast to the 1.4% *contraction* for the bare surface. At the empty site of the half-covered surface, the interlayer spacings are close to the bare-surface values, indicating that the perturbation caused by the adsorbate is fairly localized. The adsorption energy per molecule of the $\theta=1$ system is about half that of the $\theta=0.5$ system. This weaker binding is also reflected in the 1.6% longer C–Cu_1 bond length. Interestingly, even though the $\theta=1$ adsorption bond is weaker, our calculations show that this system is stable by 0.15 eV/CO relative to the half-covered surface and a free CO molecule. While this does *not* necessarily mean that the $\theta=1$ system is stable overall, it does suggest that the maximum coverage is greater than 0.5. This is consistent with the experimental observation of a $\theta=0.57$ saturation coverage of CO on copper (001).

Finally, a recent investigation using classical potentials suggested that the ideal $\theta=0.5$ structure is unstable with respect to a cell-doubling distortion along the x direction.[55] In this proposed reconstruction, alternating rows of adsorbates parallel to the y axis tilt toward the $+y$ and $-y$ azimuths, respectively. We have tested this claim within the LDA by making small, finite distortions along the proposed reconstruction coordinate, and have found that the energy actually *increases* markedly relative to the ideal structure, contrary to the classical-potential study.

VI. VIBRATIONAL ANALYSIS

A. Force constants

Vibrational states of the coupled adsorbate-substrate system are determined from first principles within a harmonic force-constant model. No *a priori* assumptions are made regarding the nature of the modes, and atoms of both the adlayer and the substrate are treated on an equal footing. The normal modes of vibration are obtained by solving the generalized eigenvalue problem,

$$\mathbf{K}\cdot x=-\omega^2\mathbf{M}\cdot x, \tag{1}$$

where the eigenvector x resides in the $3N$-dimensional configuration space of the N atoms, with origin at the equilibrium configuration, the eigenvalue ω^2 is the square of the normal-mode frequency, $\mathbf{M}$ is the diagonal $3N\times 3N$ matrix of atomic masses, and $\mathbf{K}$ is the symmetric $3N\times 3N$ matrix of harmonic force constants (i.e., the matrix of second derivatives of the energy with respect to atomic coordinates). In this study, we consider vibrational modes at the $\bar{\Gamma}$ point (i.e., the center) of the $(\sqrt{2}\times\sqrt{2})R45°$ SBZ.

The force constants are obtained through a series of LDA calculations. Starting from the equilibrium configuration, a given atom in the unit cell is displaced by a small amplitude in a given direction, and the resulting force distribution is computed. This procedure is repeated for several small displacements of the atom, and the force constants coupling to this degree of freedom are given by the linear dependence of the forces on the displacement amplitude: $\mathbf{K}_{ij}=-\partial F_j/\partial x_i=\partial^2 U/\partial x_i\partial x_j$, where i and j are composite indices specifying both atom and polarization and U is the total energy. Each row of the force constant matrix is computed similarly. It is worth noting that these force constants are not interatomic force constants, since lattice periodicity is maintained and a whole sublattice of atoms is displaced. They are more properly referred to as lattice force constants.

By symmetry, force constants $\mathbf{K}_{ij}$ and $\mathbf{K}_{ji}$ should be equal for all i and j. However, since they are computed separately, the extent to which these matrix elements differ gives a check on the precision of the method. For our calculations, the symmetry error of the computed force constants is of order 0.1% of the largest force constant, or smaller. Before solving for the normal modes, the force constant matrix is symmetrized by averaging it with its transpose.

Another check on the precision of the method is the extent to which the computed force constants obey the acoustic sum rule,[56] which states that the sum of force constants of any given polarization across any row of the force-constant matrix must vanish. This rule expresses the fact that a uniform translation of the crystal as a whole requires no work, i.e., the space in which the lattice resides is translationally invariant. We find, however, that the acoustic sum rule is violated in our calculations by as much as 0.5% of the largest force constant. We have determined that the principal cause of this violation is that the discreteness of the fast Fourier transform (FFT) grid in the unit cell breaks translational invariance, and thus the lattice has a small but nonnegligible anomalous restoring force against uniform translations away from a preferred position. In order to obtain a physically reasonable vibrational spectrum, it is necessary to enforce the acoustic sum rule by making small adjustments to the force constants. Since the error is small and involves long-wavelength motion, the correction has no noticeable effect on the vibrational spectrum except at very low frequencies below about 4 cm^{-1}. Since there is no unique way to make the appropriate adjustments to the force constants, we have tried several reasonable schemes and have found that they all have essentially the same largely negligible effect on the spectrum.

In Sec. IV we showed that a seven-layer copper slab is sufficiently thick to give the correct surface structure. However, it is clear that this model is *not* sufficient to describe the coupled lattice dynamics of an adsorbed substrate. Bulk modes, for example, cannot be accommodated by such a model, and we show below that their inclusion is essential for a correct description of the low-frequency adsorbate dynamics. Furthermore, even modes localized at a surface often

TABLE X. First-principles force constants of both z and x polarization for bulk copper and the bare copper (001) surface in units of eV/Å^2.

Atom	Bulk		Bare surface			
	Cu_1		Cu_1		Cu_2	
Polarization	z	x	z	x	z	x
Cu_1	8.12	8.18	5.18	5.73	−2.27	−2.40
Cu_1'	0.34	−4.12	−0.50	−3.49	−2.27	0.16
Cu_2	−2.04	−2.06	−2.27	−2.40	8.17	8.29
Cu_2'	−2.04	0.04	−2.27	0.16	0.52	−4.07
Cu_3	−0.11	0.01	−0.10	0.04	−2.01	−1.98
Cu_3'	−0.08	−0.02	−0.10	−0.04	−2.01	0.02
Cu_4	0.02	−0.01	0.03	−0.01	−0.11	0.02
Cu_4'	0.02	0.01	0.03	0.00	−0.08	−0.04

penetrate further than the dimensions of the thin slab model. On the other hand, to perform the force-constant analysis described above on a sufficiently thick slab would be computationally prohibitive. To remedy this difficulty, we take advantage of the fact that, even though the excitations themselves are long ranged, the coupling constants are not. In particular, thin-slab calculations give the correct force constants for the copper (001) surface. The electrons in the metal rapidly screen out the presence of the surface, so that the force constants converge to their bulk values within about three atomic layers. In a separate calculation, we compute lattice force constants for bulk copper, and then use the two sets of calculations to construct the force-constant matrix for a much thicker slab.[57] Since all bulk layers interact with their neighbors in exactly the same way, we can pad the interior of the thin slab with an arbitrary number of bulk layers with no additional computational effort. The vibrational spectra reported in this article are computed for *effective slabs* constructed with 2000 additional copper layers.

Tables X and XI contain the computed $\bar{\Gamma}$-point force constants in eV/Å^2 for bulk copper and for the bare, half-covered, and fully covered copper (001) surface. In all cases, the calculations have been carried out on unit cells with two (001) sites per layer in $(\sqrt{2}\times\sqrt{2})R45°$ symmetry. Even though this pattern is strictly required only for the half-

TABLE XI. First-principles force constants of both z and x polarization for the half-covered and fully covered copper (001) surface in units of eV/Å^2.

Atom	O		C		Cu_1		Cu_1'	
Polarization	z	x	z	x	z	x	z	x
Half-covered surface								
O	110.44	0.90	−108.30	−1.53	−1.24	0.43	−0.94	0.15
C	−108.30	−1.53	119.34	2.77	−11.32	−0.84	1.00	−0.26
Cu_1	−1.24	0.43	−11.32	−0.84	17.13	6.06	−0.02	−3.91
Cu_1'	−0.94	0.15	1.00	−0.26	−0.02	−3.91	4.27	6.24
Cu_2	0.02	0.10	−0.38	−0.35	−2.20	−1.70	−2.08	0.09
Cu_2'	0.02	−0.05	−0.38	0.20	−2.20	−0.06	−2.08	−2.31
Cu_3		0.02	0.02	−0.08	−0.11	0.72	−0.08	−0.05
Cu_3'		−0.02	0.02	0.08	−0.08	−0.06	−0.11	0.04
Cu_4				−0.03	0.02	0.02	0.02	−0.01
Cu_4'				0.03	0.02	−0.02	0.02	0.01
Fully covered surface								
O	109.18	4.05	−106.69	−0.91	−1.23	0.18		
O′	4.96	−1.95	−6.56	−1.86	0.30	0.43		
C	−106.69	−0.91	115.06	3.93	−9.99	−0.04		
C′	−6.56	−1.86	8.90	0.02	−0.26	−0.93		
Cu_1	−1.23	0.18	−9.99	−0.04	14.67	6.28		
Cu_1'	0.30	0.43	−0.26	−0.93	0.58	−4.23		
Cu_2	0.02	0.08	−0.25	−0.27	−1.96	−1.52		
Cu_2'	0.02	−0.01	−0.25	0.07	−1.96	−0.14		
Cu_3		0.02	0.02	−0.04	−0.11	0.09		
Cu_3'		−0.02	0.02	0.04	−0.08	−0.12		
Cu_4				0.02	0.02	0.05		
Cu_4'				−0.02	0.02	−0.05		

covered surface, we have used it for all systems in order to facilitate comparisons. Tetragonal symmetry permits the force-constant matrices to be decoupled into three independent blocks, one block describing motion perpendicular to the (001) plane (z polarized), and two degenerate blocks describing parallel motion (x and y polarized). The force-constant tables are arranged so that the displaced coordinate is listed along the top and the responding coordinate is listed along the side. For the surfaces, the atoms are labeled according to the convention of Fig. 1, with the two distinct in-plane sites distinguished by a prime. For the bulk, since all layers are equivalent, each layer is numbered relative to the one containing the displaced atom. For all but the half-covered surface, the primed and unprimed sites are equivalent by symmetry. Therefore force constants associated with motion of primed atoms can be deduced from those of unprimed atoms.

A comparison of the bulk and bare-surface force constants in Table X reveals several important features. We see, for example, that the range of the coupling is about three layers. At this distance, the lattice force constants are less than 1% of their largest value, which is small enough to have only a negligible effect on the vibrational spectrum. In addition, by the third layer into the surface, the force constants have converged to their bulk values. These two results give further justification for the use of a seven-layer slab. Table X also shows that only displacements of the outermost copper layer are needed in computing surface force constants. The last two columns, obtained by displacing Cu_2, give redundant information. The Cu_2–Cu_1 and Cu_2–Cu_1' coupling constants are identical to the Cu_1–Cu_2 and Cu_1–Cu_2' values, as is required by symmetry. Furthermore, the restoring force on Cu_2 and its coupling to atoms in the same and deeper layers are very close to their corresponding bulk values (e.g., Cu_2–Cu_2 for the surface is very similar to Cu_1–Cu_1 in the bulk). Based on this result for the bare surface, we have chosen not to displace the second and deeper layers in computing surface force constants for the covered surfaces.

The comparison between bulk and the bare surface also shows that the coupling is stronger near the surface. On examining the Cu_1–Cu_1' and Cu_1–Cu_2 force constants for both x and z polarizations, we find that all but the x-polarized Cu_1–Cu_1' force constants strengthen at the surface. This enhancement, especially of the z-polarized couplings, is consistent with the inward structural relaxation at the surface.

Force constants for the half-covered and fully covered surfaces are compared in Table XI. These data show that the change in coverage has a much more significant impact on the x-polarized couplings than on the z-polarized couplings. For example, the in-plane oxygen restoring force is over four times as large at full coverage as at half coverage, whereas the perpendicular restoring force changes by only 1%. This behavior can be easily understood since an in-plane distortion moves the oxygen atom towards an adsorbate at full coverage but a vacancy at half coverage, whereas a perpendicular distortion moves the atom towards vacuum for both coverages. The force constants also provide information about the coverage dependence of the bonding. For example, the decrease in the z-polarized O–C and C–Cu_1 force constants indicates a weakening of the intramolecular and adsorption bonds, respectively, with increasing coverage. The latter result is consistent with the adsorption bond energies reported in Table IX.

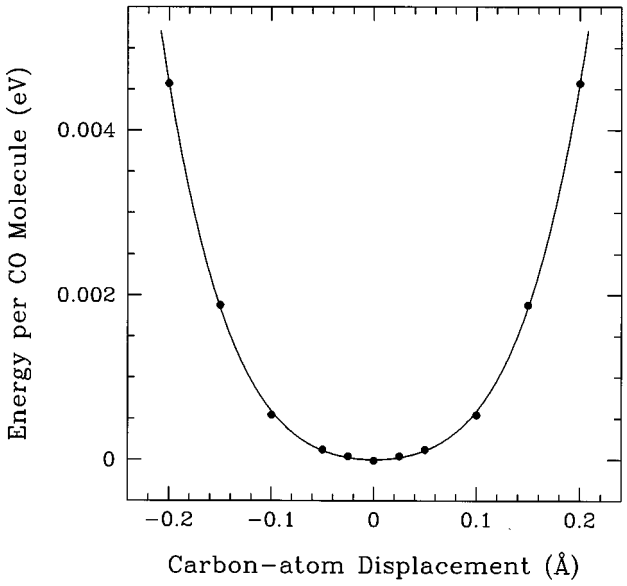

FIG. 2. Total energy of the $\theta=0.5$ system as a function of frustrated translational amplitude over a range of values accessible at experimental temperatures ($\sim$100 K). The amplitude is reported as the displacement in Å of the carbon atom away from its equilibrium position. The solid line is a quartic fit of the data (dots).

It is known from helium atom scattering (HAS) data that the in-plane frustrated translational (FT) motion of CO on copper exhibits strong quartic anharmonicity.[58] Since one of the goals of this work is to understand the observed relaxation dynamics of this mode, it is critical that we describe it as accurately as possible. However, to incorporate anharmonic effects systematically throughout the vibrational analysis would be an intractable and, as we will show, unnecessary complication. The principal anharmonic part of the potential comes from a term quartic in the FT amplitude. Since no other modes are involved, the dominant effect of this term is to shift the FT frequency. We can account for this shift entirely within a harmonic framework by suitably adjusting the relevant force constants. The x-polarized C–O, C–C, and O–O force constants reported in Table XI for the half-covered surface have been adjusted according to the prescription described below to reflect the shifted frequency. Since the fully covered surface is, at present, hypothetical, we have not carried out the lengthy anharmonic calculations required to adjust its force constants.

In order to determine the anharmonic shift of the FT frequency, we need to map out the total energy as a function of FT amplitude. This requires knowing the mode's atomic displacement pattern, which is obtained by solving Eq. (1) using the unadjusted force-constant matrix. For reasons that will become apparent in Sec. VI B, there is some ambiguity in isolating the FT coordinate directly. Thus, for the purposes of mapping out its potential, we have defined the FT coordinate to be localized on the CO molecule and orthogonal to the (uniquely specified) frustrated rotational (FR) mode. Fig-

ure 2 shows the dependence of the total energy on FT amplitude over a range of values accessible at experimental temperatures (~100 K). The dots in Fig. 2 are the computed points, and the solid line is the following quartic fit:

$$E(x_C) = 0.0203x_C^2 + 0.9237x_C^4, \tag{2}$$

where x_C is the carbon-atom displacement in Å, and E is the energy per CO molecule in eV. We solve for the ground and first-excited states of this potential by numerically integrating the Schrödinger equation and find a frequency of $\nu = (E_1 - E_0)/h = 27\,\mathrm{cm}^{-1}$. In contrast, if we had truncated Eq. (2) at quadratic order, the frequency would have been 14 cm^{-1}, thus demonstrating the importance of anharmonicity here. The in-plane C–O, C–C, and O–O force constants are now adjusted to reflect the anharmonically shifted frequency. The FR atomic displacement pattern and the acoustic sum rule provide the two remaining constraints necessary to uniquely specify the adjustment. Quantitatively, the effect on this 2×2 portion of the force-constant matrix is

$$\begin{pmatrix} 0.99 & -1.62 \\ -1.62 & 2.70 \end{pmatrix} \rightarrow \begin{pmatrix} 0.90 & -1.53 \\ -1.53 & 2.77 \end{pmatrix}. \tag{3}$$

Note that this procedure can account for temperature-dependent FT properties since the frequency depends on the range over which the anharmonic potential is sampled.

B. Vibrational spectra

Vibrational spectra are obtained from the computed force constants by solving Eq. (1) for the 2000 layer effective slab. Since slab models are finite, the resulting vibrational spectra are discrete, even though the spectrum of a truly infinite substrate would have a continuum of bulk-like modes. To simulate this behavior, we have convoluted our discrete spectra with a Gaussian of unit area and 0.25 cm^{-1} width. This smoothing makes the spectra easier to interpret, and, since the effective slabs are chosen to be quite large, we have been able to use a fairly narrow smoothing function. In computing natural linewidths of spectral features, we filter out the broadening effect of the smoothing function.

The force-constant calculations reported in Sec. VI A all maintain the in-plane lattice periodicity of the $(\sqrt{2}\times\sqrt{2})R45°$ surface unit cell, i.e., displacements of corresponding atoms in different unit cells are in phase. Thus the resulting vibrational spectra shown below contain modes at the $\bar{\Gamma}$ point of the SBZ. Since the $(\sqrt{2}\times\sqrt{2})R45°$ cell is not primitive for the bare and fully covered surfaces, the computed vibrational spectra for these systems contain modes at both the $\bar{\Gamma}$ and $\bar{M}$ points of their primitive SBZ. These points both map to the $\bar{\Gamma}$ point of the folded SBZ.

Figures 3(a) and 3(b) exhibit the vibrational density of *z*- and *x*-polarized modes, respectively, as a function of frequency for the bare copper (001) surface. The perpendicular spectrum in Fig. 3(a) consists of a broad band of modes below 263 cm^{-1} and three sharp features labeled $A-C$. We identify the nature of the modes by examining their atomic displacement patterns, obtained from the solution of Eq. (1). The broad band corresponds to bulk copper phonon modes that project onto the $\bar{\Gamma}$ point of the bare SBZ. These include

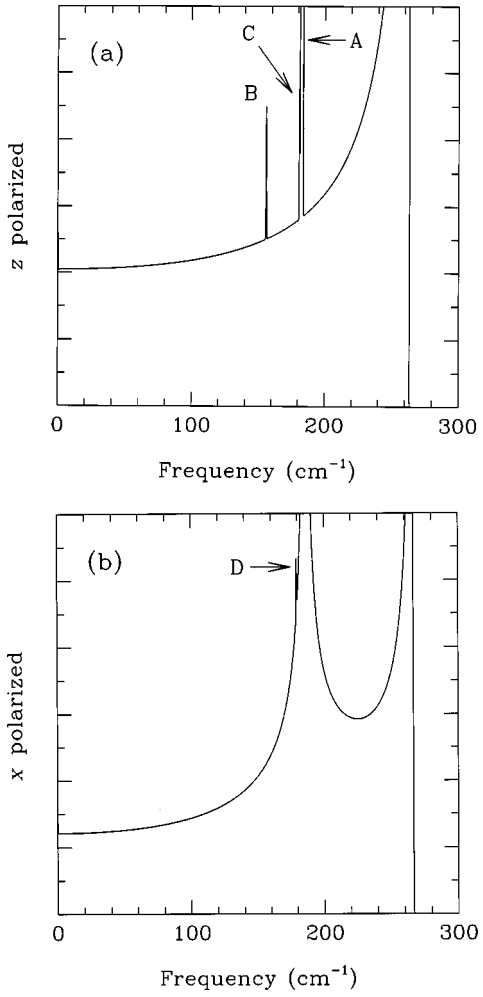

FIG. 3. Density of (a) *z*-polarized and (b) *x*-polarized vibrational states vs frequency for the bare copper (001) surface. The spectrum includes modes at the $\bar{\Gamma}$ point of the surface Brillouin zone for the $\sqrt{2}\times\sqrt{2}R45°$ surface unit cell.

longitudinal acoustic phonons along the path $\Gamma\rightarrow X$ in the fcc BZ. The band edge at 263 cm^{-1} compares reasonably well with the experimental value of 242 cm^{-1}.[59] Feature *A*, at around 182 cm^{-1}, corresponds to the bulk phonons for modes that project onto the $\bar{M}$ point of the bare SBZ. This band consists of phonon modes along the path $X\rightarrow W$ in the fcc BZ, and is known experimentally to be very narrow (165–171 cm^{-1}).[59] Features *B* and *C* are the S_1 and S_2 surface modes,[60] respectively, at the $\bar{M}$ point of the bare SBZ. The S_1 mode is a Rayleigh wave, and its computed frequency is 156 cm^{-1}, about 14% larger than the measured value of 137 cm^{-1}.[61] For the S_2 mode, odd-numbered atomic layers, counting from the surface, are stationary. The even-numbered layers are in motion, with maximum amplitude on the second layer and exponential penetration depth of 1.4 layers. The computed (181 cm^{-1}) and experimental (163 cm^{-1}) (Ref. 60) frequencies again agree at the 10%–15% level.

In the *x*-polarized spectrum shown in Fig. 3(b), the two broad bands of modes below and above 186 cm^{-1} correspond to bulk copper phonons that project onto the $\bar{\Gamma}$ and $\bar{M}$ points, respectively, of the bare SBZ. The band edges at 186

TABLE XII. Summary of vibrational spectral features for the bare, half-covered, and fully covered copper (001) surface. For the fully covered surface, modes are distinguished as coming from either the $\overline{\Gamma}$ or $\overline{M}$ point of the unfolded primitive surface Brillouin zone. Frequencies and linewidths are given in cm^{-1}, and lifetimes are given in ps.

Mode	Bare		Half covered		Fully covered	
	Theory	Experiment	Theory	Experiment	$\overline{\Gamma}$	$\overline{M}$
Molecular bond stretching			2111	2085[a]	2154	2019
Adsorption bond stretching			427	345[b]	402	391
Rayleigh wave, S_1						
Frequency, ν	156	137[c]	129	123[d]		64
Linewidth, $\Delta\nu$	0		1.0			0
Lifetime, τ	∞		5.2			∞
S_2 surface mode	181	163[e]	187			184
Frustrated rotation			282	285[b]	353	280
Frustrated translation						
Frequency, ν			27	32[d]	43	340
Linewidth, $\Delta\nu$			1.8		7.5	0
Lifetime, τ			3.0	2.3 ± 0.4[f]	0.7	∞
L_1 surface mode	179					

[a]Reference 54.
[b]Reference 2.
[c]Reference 61.
[d]Reference 6.
[e]Reference 60.
[f]Reference 5.

and 266 cm^{-1} compare favorably with the experimental values of 171 and 242 cm^{-1}, respectively.[59] The sharp feature labeled D is the L_1 longitudinal surface phonon first identified in Ref. 60. This mode has large in-plane displacements at the surface which decay exponentially into the bulk with a characteristic length of 1.94 layers. The computed frequency, 179 cm^{-1}, is in good agreement with the previously reported value, 167 cm^{-1}.[60] Table XII summarizes the spectral features of the bare (001) surface, as well as those of the half-covered and fully covered surfaces.

The z-polarized vibrational spectra of the half-covered and fully covered surfaces are compared in Figs. 4(a) and 4(b), respectively. The spectra for both coverages exhibit the same bulk features seen in the bare-surface spectrum. In addition, these spectra both contain S_1 and S_2 peaks; these features are found to be coverage dependent. The frequency of the Rayleigh mode [labeled B' and B'' in Figs. 4(a) and 4(b), respectively] is strongly coverage dependent, going from 156 to 129 to 64 cm^{-1} as the CO coverage increases from $\theta=0$ to 0.5 to 1. This decrease in frequency is primarily the result of mass loading of the surface and not changes in coupling strength due to adsorption. We know this is true because the surface copper atom and its attached CO molecule move together as a unit.

For the bare and fully covered surfaces, the Rayleigh wave is a sharp, solitary mode. However, our calculations predict that, for the half-covered surface, this mode broadens into a peak of finite width. The explanation for this unexpected result is that the reduced in-plane translational symmetry of this system permits resonant mixing between the S_1 mode and bulk phonons at the $\overline{\Gamma}$ point of the underlying bare SBZ. This coupling, which is symmetry forbidden in the primitive (001) unit cells of the other two systems, causes the S_1 mode to broaden into a resonance peak. To illustrate its effect, Figs. 5(a) and 5(b) compare the normal coordinates of the central S_1 mode at half coverage to the solitary S_1 mode

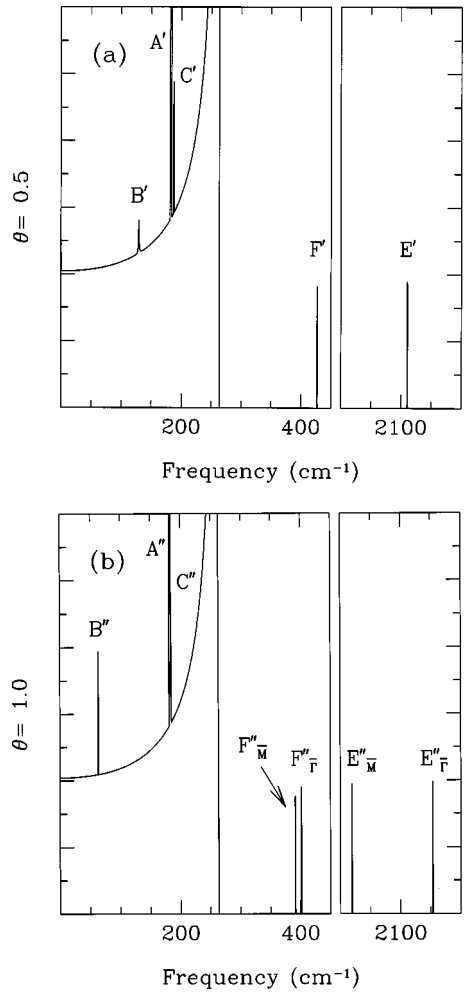

FIG. 4. Density of z-polarized vibrational states vs frequency for a CO overlayer on the copper (001) surface at (a) half and at (b) full coverage. The spectrum includes modes at the $\overline{\Gamma}$ point of the surface Brillouin zone for the $\sqrt{2}\times\sqrt{2}R45°$ surface unit cell.

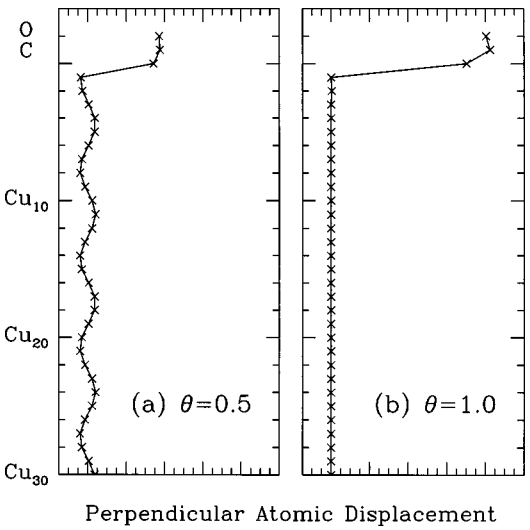

FIG. 5. Comparison of the atomic displacement patterns for (a) the normal mode at the center of the S_1 (Rayleigh) resonance peak at half coverage [feature B' in Fig. 4(a)] and (b) the solitary S_1 normal mode at full coverage [feature B'' in Fig. 4(b)]. The horizontal axis gives the relative atomic displacements for these *z*-polarized modes, and the vertical axis labels the atomic layers. For clarity only a portion of the full 2000 layer slab is displayed.

at full coverage. Modes in the resonance-broadened peak exhibit large-amplitude S_1-like surface atomic motions, but also possess an admixture of bulk-phonon character which penetrates throughout the bulk. As a result, a surface-localized mode can only be obtained by superposing normal modes in the resonance peak. Since these normal modes propagate in time with different frequencies, the prepared disturbance will eventually decay on a time scale set by the width of the peak. After filtering out the effect of the Gaussian smoothing function, the natural linewidth of the S_1 resonance is 1.0 cm^{-1}, which corresponds to a lifetime of 5.2 ps. This mode has been observed for the half-covered surface in a HAS experiment at a frequency of 123 cm^{-1}.[6] To our knowledge, its lifetime has not been measured.

The S_2 mode [labeled C' and C'' in Figs. 4(a) and 4(b), respectively] is only weakly coverage dependent. Since the adlayer and the outermost copper layer are stationary for this mode, coverage dependence is mediated through the interaction of the CO molecules with the second copper layer, which, as we saw in Sec. VI A, is small. This is also the reason why the S_2 mode of the half-covered surface does not resonantly couple to bulk $\overline{\Gamma}$ phonons, as does the S_1 mode, even though this coupling is permitted by the reduced translational symmetry.

The spectra in Fig. 4 possess additional modes at frequencies above the bulk-phonon band edge. They primarily involve carbon and oxygen motion, and therefore are not present in the bare-surface spectrum. Features E' and F' in the $\theta=0.5$ spectrum constitute the C–O and C–Cu bond-stretching modes, respectively. For the former mode, the oxygen and carbon atoms move in opposite directions perpendicular to the surface, with the CO center of mass and all copper atoms remaining essentially stationary. The computed frequency, 2111 cm^{-1}, compares very favorably with the experimental value, 2085 cm^{-1}.[54] For the latter mode, the CO molecule moves as a unit in opposition to the copper atom to which it is attached. Here the CO–Cu center of mass remains largely fixed, as do the remaining copper atoms, although there is slightly greater penetration of this mode into the surface. The computed frequency, 427 cm^{-1}, is in only fair agreement with the measured value, 345 cm^{-1}.[2] This discrepancy is largely due to our choice of coordinates used in computing the *z*-polarized force constants. Since the C–O bond is very strong, the CO molecule moves essentially as a unit for all but the molecular bond-stretching mode. Individual motion of either the carbon or oxygen atoms leads to a huge restoring force, resulting in huge C–O, C–C, and O–O force constants. Thus, computing the energy in this coordinate system of a mode in which the carbon and oxygen atoms move together involves the subtraction of large numbers to obtain a small number. Because of the concomitant numerical instability, it would have been better to choose a different coordinate system for computing force constants, one in which the O and C degrees of freedom are replaced with their symmetric and antisymmetric combinations. Test calculations in which we vary the C–O, C–C, and O–O force constants by a small amount give CO–Cu stretch frequencies as low as about 390 cm^{-1}. Implementing the improved coordinate system in the present study would have been computationally very demanding, and, in our opinion, unwarranted in light of the reasonably good results already in hand. In future studies of adsorbate vibrational dynamics, however, we plan to adopt the new approach.

Since the fully covered surface contains one additional CO molecule per unit cell, there are two additional modes in the *z*-polarized spectrum. The features labeled $E''_{\overline{\Gamma}}$ and $E''_{\overline{M}}$ are molecular bond-stretching modes with $\overline{\Gamma}$ and $\overline{M}$ symmetry, respectively, relative to the primitive SBZ of this system. Similarly, features $F''_{\overline{\Gamma}}$ and $F''_{\overline{M}}$ are adsorption bond-stretching modes at the $\overline{\Gamma}$ and $\overline{M}$ points, respectively. The frequencies of the F'' modes are smaller than their counterpart in the half-covered surface, indicating a weakening of the adsorption bond. Furthermore, the small value of the splitting reveals a highly nondispersive mode, and suggests that dipole and other long-range interactions are not important for this degree of freedom. For the E'' modes, on the other hand, the splitting is very large. It is known that long-range dipole interactions are important for the C–O stretch mode and lead to a dispersive band. Since the fully covered surface is, at present, hypothetical, the vibrational frequencies reported in Table XII for this system are not compared to experiment.

Figures 6(a) and 6(b) show the *x*-polarized vibrational spectra for the half-covered and fully covered surfaces, respectively. In addition to the bulk-phonon band below 266 cm^{-1}, these spectra contain new modes associated with the carbon and oxygen in-plane degrees of freedom. The mode labeled G' at 282 cm^{-1} in the $\theta=0.5$ spectrum involves motion of the carbon and oxygen atoms in opposite directions, with the C–O center of mass essentially fixed over the adsorption site and negligible penetration of the mode into the copper substrate. This ''rocking'' motion defines the frustrated rotational mode, and its computed frequency

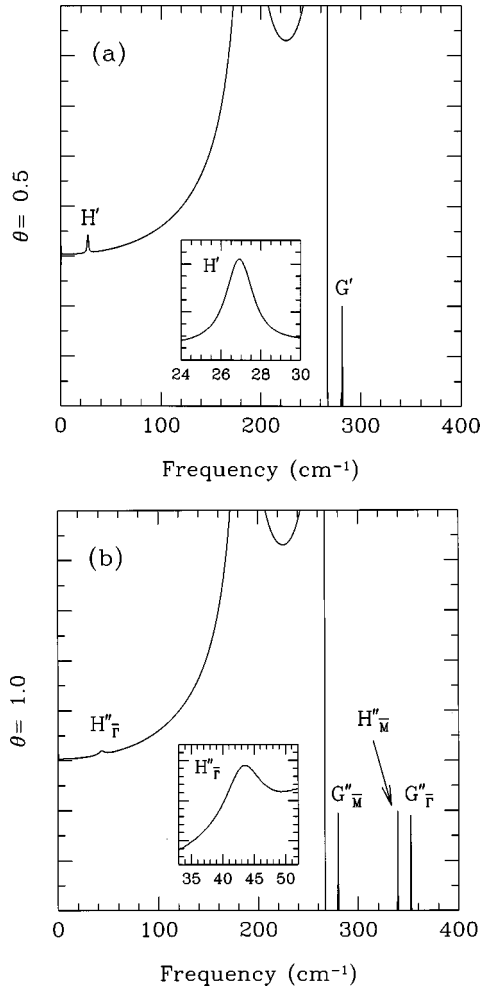

FIG. 6. Density of *x*-polarized vibrational states vs frequency for a CO overlayer on the copper (001) surface at (a) half and at (b) full coverage. The spectrum includes modes at the $\bar{\Gamma}$ point of the surface Brillouin zone for the $\sqrt{2}\times\sqrt{2}R45°$ surface unit cell. The inset in each panel highlights the frustrated translational resonance peak.

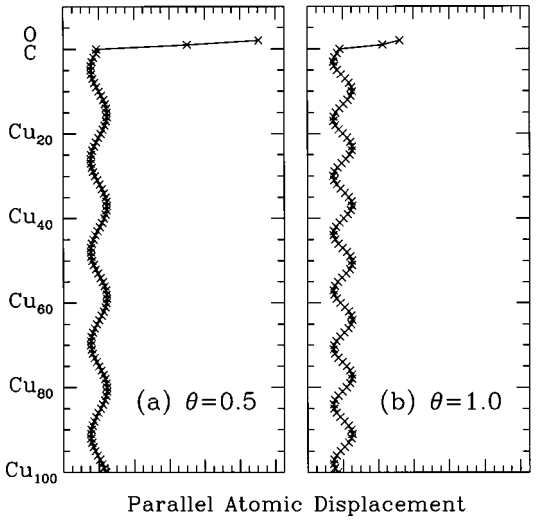

FIG. 7. Comparison of the atomic displacement patterns for normal modes at the center of the frustrated translational resonance peak at (a) half coverage [feature H' in Fig. 6(a)] and at (b) full coverage [feature $H''_{\bar{\Gamma}}$ in Fig. 6(b)]. The horizontal axis gives the relative atomic displacements for these *x*-polarized modes, and the vertical axis labels the atomic layers. For clarity only a portion of the full 2000 layer slab is displayed.

agrees very closely with the 285 cm^{-1} experimental value.[2] In the $\theta=1$ spectrum there are two FR modes: one at 353 cm^{-1} in which the two CO molecules rock in phase (labeled $G''_{\bar{\Gamma}}$), and the other at 280 cm^{-1} in which they rock 180° out of phase (labeled $G''_{\bar{M}}$).

The other in-plane degree of freedom associated with the adsorbate is the frustrated translational, or ''wagging,'' mode, in which the carbon and oxygen atoms oscillate in the same direction about the binding site. In Sec. VI A we saw that this anharmonic mode has a frequency of 27 cm^{-1} for the half-covered surface at the temperature range of interest. This computed frequency is in excellent accord with the 32 cm^{-1} HAS measurement of Ref. 6. Since the FT frequency is well within the bulk-phonon continuum, it can mix with phonons at the same frequency and broaden into a resonance peak of finite spectral width, in the same manner as described above for the Rayleigh mode of this system. This resonance peak, labeled H' in Fig. 6(a), has a natural linewidth of 1.8 cm^{-1}, which corresponds to a lifetime of 3.0 ps. This prediction is in excellent quantitative agreement with the 2.3 ± 0.4 ps FT relaxation time measured for this system at 100 K,[5] and thus provides an explanation of the observed rapid damping of this mode. Frustrated translations decay via resonant coupling to long-wavelength substrate phonons. This is a purely harmonic mechanism, involving no higher-order effects such as anharmonic vibrational coupling or electron–phonon coupling. These other mechanisms are expected to contribute at much longer time scales, and therefore are subdominant. Recently, we developed an analytical theory of resonant damping of adsorbate vibrational motion[62] which predicts FT lifetimes in good agreement with both experiment and the present computation, thus reinforcing our interpretation.

At full coverage, there are two FT modes in the spectrum in Fig. 6(b), one at the $\bar{\Gamma}$ point of the primitive (001) SBZ and the other at the $\bar{M}$ point. The calculations show that the FT band is *highly* dispersive. The $\bar{\Gamma}$ mode (labeled $H''_{\bar{\Gamma}}$) is at 43 cm^{-1}, in the frequency range of long-wavelength bulk phonons, whereas the $\bar{M}$ mode (labeled $H''_{\bar{M}}$) is at 340 cm^{-1}, well above the bulk band edge and even interleaving the FR modes. Some degree of dispersion is expected, since, for the $\bar{M}$ mode, the CO molecules wag into each other, whereas at $\bar{\Gamma}$ they move in phase. However, the magnitude of the bandwidth is entirely unexpected; HAS experiments on the half-covered surface find a FT bandwidth of only 14 cm^{-1}.[6] Since the FT mode at 43 cm^{-1} and the phonons in that frequency range both have $\bar{\Gamma}$ symmetry relative to the primitive SBZ, resonant coupling between the adlayer and substrate is permitted, just as it is for the half-covered surface. This coupling is significantly stronger at the higher coverage. The spectral width of the $H''_{\bar{\Gamma}}$ resonance is 7.5 cm^{-1}, which corresponds to a lifetime of 0.7 ps. These results are in accord with our analytical theory,[62] in which the damping rate depends linearly on coverage and quadratically on frequency. Figures 7(a) and 7(b) illustrate the normal-

mode displacement pattern at the center of the FT resonance for the half-covered and fully covered surfaces, respectively. The shift in resonant frequency is indicated by the different wavelengths of the bulk-phonon part of the modes, and the enhanced coupling at higher coverage can be seen qualitatively in the decreased ratio of FT amplitude to bulk-phonon amplitude in the normal coordinate.

VII. CONCLUSIONS

We have carried out a comprehensive first-principles investigation of the structural and vibrational properties of CO on copper (001), a prototype chemisorbed metal surface. To examine the coverage-dependent behavior, we have considered CO adlayers at three different coverages: $\theta=0$, 0.5, and 1. All computed structural and vibrational properties agree well with the available experimental measurements. The structural and force-constant analyses reveal a weakening of the chemisorption bond on going from half to full coverage. Nevertheless, we find that the fully covered surface is energetically favorable to the half-covered surface plus free CO molecule. While this does not necessarily imply overall stability of the $\theta=1$ phase, it does suggest that the maximum stable coverage is greater than $\theta=0.5$, in agreement with experiment.

Our vibrational analysis of these systems has revealed several striking features in the spectra. First, the low-frequency, in-plane frustrated translational motion of the CO molecules exists not as a normal mode of the system, but, rather, as a broad resonance peak of finite lifetime. The normal modes in this peak are a combination of FT motion and long-wavelength bulk copper phonon motion, illustrating the resonant coupling between these two types of modes. The predicted lifetime of 3.0 ps for the half-monolayer system is in excellent agreement with the experimental value of 2.3 ± 0.4 ps, thus demonstrating that this resonant damping mechanism dominates the relaxation dynamics of this mode.

In addition we find that, for the $\theta=0.5$ system, the mode corresponding to the zone-boundary Rayleigh wave of the underlying copper (001) surface also resonantly couples to the substrate phonons and develops a finite lifetime. From the spectrum we have computed, we predict, in advance of experiment, a characteristic decay time of 5.2 ps. This resonance-broadening effect is not seen at $\theta=1$. The reason for the differing behavior is that the two coverages possess different in-plane translational symmetry. Resonant mixing is permitted in the reduced symmetry of the $\theta=0.5$ system, but is symmetry forbidden at $\theta=1$.

ACKNOWLEDGMENTS

Financial support for this research was provided by the National Science Foundation under Grant No. DMR 97-02514, by the Petroleum Research Fund of the American Chemical Society under Grant No. 32007-G5, and by the Laboratory for Research on the Structure of Matter at the University of Pennsylvania. Computational support was provided by the San Diego Supercomputer Center.

[1] G. A. Somorjai, *Introduction to Surface Chemistry and Catalysis* (Wiley, New York, 1994).
[2] C. J. Hirschmugl, G. P. Williams, F. M. Hoffmann, and Y. J. Chabal, Phys. Rev. Lett. **65**, 480 (1990); J. Electron Spectrosc. Relat. Phenom. **54/55**, 109 (1990); C. J. Hirschmugl, Y. J. Chabal, F. M. Hoffman, and G. P. Williams, J. Vac. Sci. Technol. A **12**, 2229 (1994).
[3] M. Morin, N. J. Levinos, and A. L. Harris, J. Chem. Phys. **96**, 3950 (1992).
[4] E. Borguet and H.-L. Dai, Chem. Phys. Lett. **194**, 57 (1992); J. Chem. Phys. **101**, 9080 (1994); J. Dvorak, E. Borguet, and H.-L. Dai, Surf. Sci. **369**, L122 (1996).
[5] T. A. Germer, J. C. Stephenson, E. J. Heilweil, and R. R. Cavanagh, Phys. Rev. Lett. **71**, 3327 (1993); J. Chem. Phys. **101**, 1704 (1994).
[6] J. Ellis, J. P. Toennies, and G. Witte, J. Chem. Phys. **102**, 5059 (1995); M. Bertino, J. Ellis, F. Hofmann, J. P. Toennies, and J. R. Manson, Phys. Rev. Lett. **73**, 605 (1994).
[7] A. Graham, F. Hofmann, and J. P. Toennies, J. Chem. Phys. **104**, 5311 (1996).
[8] C. J. Hirschmugl and G. P. Williams, Phys. Rev. B **52**, 14177 (1995).
[9] L. M. Struck, L. J. Richter, S. A. Buntin, R. R. Cavanagh, and J. C. Stephenson, Phys. Rev. Lett. **77**, 4576 (1996).
[10] J. Braun, A. P. Graham, F. Hofmann, W. Silvestri, J. P. Toennies, and G. Witte, J. Chem. Phys. **105**, 3258 (1996).
[11] A. P. Graham, F. Hofmann, J. P. Toennies, G. P. Williams, C. J. Hirschmugl, and J. Ellis, J. Chem. Phys. **108**, 7825 (1998).
[12] M. Head-Gordon and J. C. Tully, J. Chem. Phys. **96**, 3939 (1992), Phys. Rev. B **46**, 1853 (1992).
[13] J. C. Tully, M. Gomez, and M. Head-Gordon, J. Vac. Sci. Technol. A **11**, 1914 (1993).
[14] M. Head-Gordon and J. C. Tully, Chem. Phys. **175**, 37 (1993).
[15] G. te Velde and E. J. Baerends, Chem. Phys. **177**, 399 (1993).
[16] P. H. T. Philipsen, G. te Velde, and E. J. Baerends, Chem. Phys. Lett. **226**, 583 (1994).
[17] C. Springer, M. Head-Gordon, and J. C. Tully, Surf. Sci. **320**, L57 (1994); C. Springer and M. Head-Gordon, Chem. Phys. **205**, 73 (1996).
[18] C. J. Hirschmugl, G. P. Williams, B. N. J. Persson, and A. I. Volokitin, Surf. Sci. **317**, L1141 (1994); A. I. Volokitin and B. N. J. Persson, JETP **81**, 545 (1995).
[19] S. P. Lewis and A. M. Rappe, Phys. Rev. Lett. **77**, 5241 (1996).
[20] S. C. Park, J. M. Bowman, and D. A. Jelski, J. Chem. Phys. **104**, 2457 (1996); S. Carter, S. J. Culik, and J. M. Bowman, *ibid.* **107**, 10458 (1997).
[21] J. C. Tracy, J. Chem. Phys. **56**, 2748 (1972).
[22] J. Pritchard, Surf. Sci. **79**, 231 (1979).
[23] S. Andersson and J. B. Pendry, Phys. Rev. Lett. **43**, 363 (1979).
[24] C. F. McConville, D. P. Woodruff, K. C. Prince, G. Paolucci, V. Chab, M. Surman, and A. M. Bradshaw, Surf. Sci. **166**, 221 (1986).
[25] P. Hohenberg and W. Kohn, Phys. Rev. **136**, B864 (1964).
[26] W. Kohn and L. J. Sham, Phys. Rev. **140**, A1133 (1965).
[27] M. J. Gillan, J. Phys.: Condens. Matter **1**, 689 (1989).
[28] M. P. Teter, M. C. Payne, D. C. Allan, Phys. Rev. B **40**, 12255 (1989).
[29] M. C. Payne, M. P. Teter, D. C. Allan, T. A. Arias, and J. D. Joannopoulos, Rev. Mod. Phys. **64**, 1045 (1992).
[30] D. M. Ceperley and B. J. Adler, Phys. Rev. Lett. **45**, 566 (1980); J. Perdew and A. Zunger, Phys. Rev. B **23**, 5048 (1981).
[31] J. P. Perdew, J. A. Chevary, S. H. Vosko, K. A. Jackson, M. R. Pederson, D. J. Singh, and C. Fiolhais, Phys. Rev. B **46**, 6671 (1992).
[32] H. Hellmann, *Einfuhrung in die Quantumchemie* (Deuticke, Leipzig, 1937); R. P. Feynman, Phys. Rev. **56**, 340 (1939).
[33] J. Ihm, A. Zunger, and M. L. Cohen, J. Phys. C **12**, 4401 (1979).
[34] W. E. Pickett, Comput. Phys. Rep. **9**, 115 (1989).
[35] D. R. Hamann, M. Schlüter, and C. Chiang, Phys. Rev. Lett. **43**, 1494 (1979).
[36] A. M. Rappe, K. M. Rabe, E. Kaxiras, and J. D. Joannopoulos, Phys. Rev. B **41**, 1227 (1990).
[37] L. Kleinman and D. M. Bylander, Phys. Rev. Lett. **48**, 1425 (1982).
[38] X. Gonze, P. Käckell, and M. Scheffler, Phys. Rev. B **41**, 12264 (1990); X. Gonze, R. Stumpf, and M. Scheffler, *ibid.* **44**, 8503 (1991).
[39] Z. W. Lu, S.-H. Wei, and A. Zunger, Phys. Rev. B **41**, 2699 (1990).
[40] M. Schlüter, J. R. Chelikowsky, S. G. Louie, and M. L. Cohen, Phys. Rev. Lett. **34**, 1385 (1975).
[41] H. J. Monkhorst and J. D. Pack, Phys. Rev. B **16**, 1748 (1977).
[42] N. D. Mermin, Phys. Rev. **137**, A1441 (1965).
[43] N. J. Ramer and A. M. Rappe (unpublished).
[44] E. C. Bain, Trans. Am. Inst. Min. Metall. Pet. Eng. **70**, 25 (1924).

[45] E. J. Walter, S. P. Lewis, and A. M. Rappe, in *Laser Techniques for Surface Science III*, Proc. SPIE 3272 (1998).
[46] Th. Rodach, K.-P. Bohnen, and K. M. Ho, Surf. Sci. **286**, 66 (1993).
[47] N. Troullier and J. L. Martins, Phys. Rev. B **43**, 1993 (1991).
[48] J. R. Chelikowsky and M. Y. Chou, Phys. Rev. B **38**, 7966 (1988).
[49] V. L. Moruzzi, J. F. Janak, and A. R. Williams, *Calculated Electronic Properties of Metals* (Pergamon, New York, 1978).
[50] C. Kittel, *Introduction to Solid State Physics*, 7th ed. (Wiley, New York, 1996).
[51] R. Hultgren, R. L. Orr, and K. K. Kelly, *Selected Values of Thermodynamic Properties of Metals and Alloys* (Wiley, New York, 1965).
[52] P. van 't Klooster, N. J. Trappeniers, and S. N. Biswas, Physica B & C **97**, 65 (1979).
[53] H. B. Gray, *Chemical Bonds: An Introduction to Atomic and Molecular Structure* (Benjamin, Menlo Park, CA, 1973), p. 98.
[54] R. Ryberg, Surf. Sci. **114**, 627 (1982).
[55] C. Springer and M. Head-Gordon (private communication, 1996).
[56] R. M. Pick, M. H. Cohen, and R. M. Martin, Phys. Rev. B **1**, 910 (1970).
[57] K. P. Bohnen and K. M. Ho, Surf. Sci. Rep. **19**, 99 (1993), and references therein.
[58] F. Hofmann and J. P. Toennies, Chem. Rev. **96**, 1307 (1996).
[59] R. M. Nicklow, G. Gilat, H. G. Smith, L. J. Raubenheimer, and M. K. Wilkinson, Phys. Rev. **164**, 922 (1967).
[60] Y. Chen, S. Y. Tong, J.-S. Kim, L. L. Kesmodel, T. Rodach, K. P. Bohnen, and K. M. Ho, Phys. Rev. B **44**, 11394 (1991).
[61] M. Wuttig, R. Franchy, and H. Ibach, Z. Phys. B **65**, 71 (1986).
[62] S. P. Lewis, M. V. Pykhtin, E. J. Mele, and A. M. Rappe, J. Chem. Phys. **108**, 1157 (1998).